COMPDYN 2011
ECCOMAS Thematic Conference on
Computational Methods in Structural Dynamics and Earthquake Engineering
M. Papadrakakis, M. Fragiadakis, V. Plevris (eds.)
Corfu, Greece, 25-28 May 2011

JOINT ESTIMATION OF STATES AND INPUT IN LINEAR STRUCTURAL DYNAMICS

Eliz-Mari Lourens[1], Geert Lombaert[1], Costas Papadimitriou[2] and Guido De Roeck[1]

[1]K.U. Leuven
Department of Civil Engineering, Kasteelpark Arenberg 40, B-3001 Leuven, Belgium
e-mail: elizmari.lourens@bwk.kuleuven.be

[2] University of Thessaly
Department of Mechanical Engineering, Volos 38334, Greece

Keywords: State estimation, Response prediction, Input estimation, Kalman filter, Force identification.

Abstract. *The problem of jointly estimating the input forces and states of a structure from a limited number of acceleration measurements is addressed. Utilizing a model-based joint input-state estimation algorithm originally developed for optimal control problems, minimum-variance unbiased estimates of the modal displacements and velocities of a structure as well as the dynamic forces causing these responses, are obtained. The proposed algorithm requires no prior information on the dynamic evolution of the input forces, is easy to implement, and allows online application. Its accuracy and effectiveness are demonstrated using data from a laboratory experiment on an instrumented steel beam and an in situ experiment on a footbridge.*

1 INTRODUCTION

In civil engineering state estimation refers to a model-based identification of quantities (e.g. displacements) that allow a complete description of the state of a structure from vibration response data. State estimators, among which the well-known Kalman filter and its variants, have been proposed for structural systems behaving both linearly and nonlinearly. A small survey is given by Ching et al. in [3]. The state estimates can be used for a variety of purposes including the prediction of stresses and fatigue loading, real-time structural health monitoring, structural control, the determination of response in critical joints, the verification of design calculations, etc. Examples include the work by Papadimitriou et al. [11], in which the Kalman filter is used as part of a methodology for estimating the damage accumulation in a structure due to fatigue from output-only vibration measurements at a limited number of locations. Ching and Beck [2] estimated the unknown states of a structure using a Kalman smoother in an application concerning reliability estimation for serviceability limit states. Smyth and Wu [15] proposed a multi-rate Kalman filter for the fusion of measured displacement and acceleration data sampled at different rates. The filter is designed to circumvent problems related to the integration of accelerometer or the differentiation of displacement data in situations where both these response quantities are available for system monitoring or damage detection. Hernandez and Bernal [9] designed a state estimator for structural dynamic systems based on the assumption that the primary source of uncertainty in the predicted state derives from errors in the matrices of the state-space model. Their estimator distinguishes itself from the related robust Kalman filter (RKF) in that it is derived on deterministic grounds, assumes no process/measurement noise and is significantly simpler to implement. It has been used as part of an iterative scheme for model updating in [7], and has been extended to nonlinear systems in [8], where it was used to estimate the states in a damaged seven-story building from a limited number of acceleration measurements.

In this contribution a joint input-state estimation algorithm is used to identify modal displacements, velocities and input forces using data from a laboratory experiment on an instrumented steel beam as well as an in situ experiment on a footbridge. The algorithm, developed by Gillijns and De Moor [6], has the structure of a Kalman filter, except that the true value of the input is replaced by an optimal estimate. It distinguishes itself from the state estimation methods mentioned above in that the excitation is assumed unknown, whilst there are also no assumptions made about its dynamic evolution (e.g. broadband, so that it can be modeled as a zero mean stationary white process). When the positions of the applied forces are known, the algorithm can be used to jointly estimate the states and input forces. Conversely, when the positions of the applied forces are unknown, a set of equivalent forces is identified. In the latter case the points of application of the forces are randomly chosen and equivalent forces, that would produce the same measured response, are identified at all chosen locations. It is this latter case, corresponding to pure state estimation in the absence of any a priori information regarding the positions or frequency characteristics of the input forces, that will be considered in this paper.

2 MATHEMATICAL FORMULATION

2.1 Equations of motion

Consider the continuous-time governing equations of motion for a linear system discretized in space:

$$\mathbf{M}\ddot{\mathbf{u}}(t) + \mathbf{C}\dot{\mathbf{u}}(t) + \mathbf{K}\mathbf{u}(t) = \mathbf{f}(t) = \mathbf{S}_{\mathrm{p}}(t)\mathbf{p}(t) \tag{1}$$

where $\mathbf{u}(t) \in \mathbb{R}^{n_{\mathrm{DOF}}}$ is the vector of displacement, $\mathbf{M}$, $\mathbf{C}$ and $\mathbf{K} \in \mathbb{R}^{n_{\mathrm{DOF}} \times n_{\mathrm{DOF}}}$ denote the mass, damping and stiffness matrix, respectively, and $\mathbf{f}(t)$ is the excitation vector. The excitation is factorized into an input force influence matrix $\mathbf{S}_{\mathrm{p}}(t) \in \mathbb{R}^{n_{\mathrm{DOF}} \times n_{\mathrm{p}}}$, and the vector $\mathbf{p}(t) \in \mathbb{R}^{n_{\mathrm{p}}}$ representing the n_{p} force time histories. Each column of the matrix $\mathbf{S}_{\mathrm{p}}$ gives the spatial distribution of the load time history in the corresponding element of the vector $\mathbf{p}$. In the case of a point load, the column of $\mathbf{S}_{\mathrm{p}}$ has only a limited number of non-zero entries corresponding to the distribution of the load over the degrees of freedom of the FE mesh. In the case of stochastic loading e.g. due to wind, the columns of the matrix $\mathbf{S}_{\mathrm{p}}$ may result from the decomposition of the load in uncorrelated contributions, e.g. by applying a Karhunen-Loève decomposition [5]. The undamped eigenvalue problem corresponding to (1) reads:

$$\mathbf{K}\boldsymbol{\Phi} = \mathbf{M}\boldsymbol{\Phi}\boldsymbol{\Omega}^2$$

where $\boldsymbol{\Phi} \in \mathbb{R}^{n_{\mathrm{DOF}} \times n_{\mathrm{DOF}}}$ collects as columns the eigenvectors $\boldsymbol{\Phi}_j$, and $\boldsymbol{\Omega}$ is a diagonal matrix containing the eigenfrequencies ω_j in $\mathrm{rad/s}$. Introducing the coordinate transformation $\mathbf{u}(t) = \boldsymbol{\Phi}\mathbf{z}(t)$ and premultiplying by $\boldsymbol{\Phi}^{\mathrm{T}}$ yields:

$$\boldsymbol{\Phi}^{\mathrm{T}}\mathbf{M}\boldsymbol{\Phi}\ddot{\mathbf{z}}(t) + \boldsymbol{\Phi}^{\mathrm{T}}\mathbf{C}\boldsymbol{\Phi}\dot{\mathbf{z}}(t) + \boldsymbol{\Phi}^{\mathrm{T}}\mathbf{K}\boldsymbol{\Phi}\mathbf{z}(t) = \boldsymbol{\Phi}^{\mathrm{T}}\mathbf{S}_{\mathrm{p}}(t)\mathbf{p}(t). \tag{2}$$

These equations can be decoupled by using the orthogonality conditions corresponding to a set of mass-normalized eigenvectors, $\boldsymbol{\Phi}^{\mathrm{T}}\mathbf{M}\boldsymbol{\Phi} = \mathbf{I}$ and $\boldsymbol{\Phi}^{\mathrm{T}}\mathbf{K}\boldsymbol{\Phi} = \boldsymbol{\Omega}^2$, and assuming proportional damping:

$$\boldsymbol{\Phi}^{\mathrm{T}}\mathbf{C}\boldsymbol{\Phi} = \boldsymbol{\Gamma}$$

where $\boldsymbol{\Gamma}$ is a diagonal matrix containing the terms $2\xi_j\omega_j$, and ξ denotes a modal damping ratio. The decoupled governing equations of motion in modal coordinates then become:

$$\ddot{\mathbf{z}}(t) + \boldsymbol{\Gamma}\dot{\mathbf{z}}(t) + \boldsymbol{\Omega}^2\mathbf{z}(t) = \boldsymbol{\Phi}^{\mathrm{T}}\mathbf{S}_{\mathrm{p}}(t)\mathbf{p}(t). \tag{3}$$

2.2 Continuous-time state-space model

By introducing the state vector $\mathbf{x}(t) \in \mathbb{R}^{n_{\mathrm{s}} \times n_{\mathrm{s}}},\ n_{\mathrm{s}} = 2n_{\mathrm{DOF}}$:

$$\mathbf{x}(t) = \begin{pmatrix} \mathbf{u}(t) \\ \dot{\mathbf{u}}(t) \end{pmatrix}$$

and utilizing the superficial identity $\mathbf{M}\dot{\mathbf{u}} - \mathbf{M}\dot{\mathbf{u}} = \mathbf{0}$, the second-order equations of motion (1) can be written as a first-order continuous-time state equation:

$$\dot{\mathbf{x}}(t) = \mathbf{A}_{\mathrm{c}}\mathbf{x}(t) + \mathbf{B}_{\mathrm{c}}\mathbf{p}(t) \tag{4}$$

where the system matrices $\mathbf{A}_{\mathrm{c}} \in \mathbb{R}^{n_{\mathrm{s}} \times n_{\mathrm{s}}}$ and $\mathbf{B}_{\mathrm{c}} \in \mathbb{R}^{n_{\mathrm{s}} \times n_{\mathrm{p}}}$ are defined as:

$$\mathbf{A}_{\mathrm{c}} = \begin{bmatrix} \mathbf{0} & \mathbf{I} \\ -\mathbf{M}^{-1}\mathbf{K} & -\mathbf{M}^{-1}\mathbf{C} \end{bmatrix},\ \mathbf{B}_{\mathrm{c}} = \begin{bmatrix} \mathbf{0} \\ \mathbf{M}^{-1}\mathbf{S}_{\mathrm{p}} \end{bmatrix}.$$

Consider next the measurement data vector $\mathbf{d}(t) \in \mathbb{R}^{n_{\mathrm{d}}}$, containing the n_{d} observed quantities expressed as a linear combination of the displacement, velocity and acceleration vectors as follows:

$$\mathbf{d}(t) = \mathbf{S}_{\mathrm{a}}\ddot{\mathbf{u}}(t) + \mathbf{S}_{\mathrm{v}}\dot{\mathbf{u}}(t) + \mathbf{S}_{\mathrm{d}}\mathbf{u}(t) \tag{5}$$

where $\mathbf{S}_\mathrm{a}$, $\mathbf{S}_\mathrm{v}$ and $\mathbf{S}_\mathrm{d} \in \mathbb{R}^{n_\mathrm{d} \times n_\mathrm{DOF}}$ are selection matrices for acceleration, velocity and displacement, respectively, in which the locations of the measurements and/or difference relations can be specified. Using equation (1) and the definition of the state vector, equation (5) can be transformed into its state-space form:

$$\mathbf{d}(t) = \mathbf{G}_\mathrm{c}\mathbf{x}(t) + \mathbf{J}_\mathrm{c}\mathbf{p}(t) \tag{6}$$

with the output influence matrix $\mathbf{G}_\mathrm{c} \in \mathbb{R}^{n_\mathrm{d} \times n_\mathrm{s}}$ and direct transmission matrix $\mathbf{J}_\mathrm{c} \in \mathbb{R}^{n_\mathrm{d} \times n_\mathrm{p}}$ defined as:

$$\mathbf{G}_\mathrm{c} = \begin{bmatrix} \mathbf{S}_\mathrm{d} - \mathbf{S}_\mathrm{a}\mathbf{M}^{-1}\mathbf{K} & \mathbf{S}_\mathrm{v} - \mathbf{S}_\mathrm{a}\mathbf{M}^{-1}\mathbf{C} \end{bmatrix}, \; \mathbf{J}_\mathrm{c} = \left[\mathbf{S}_\mathrm{a}\mathbf{M}^{-1}\mathbf{S}_\mathrm{p}\right].$$

Equations (4) and (6) together form the continuous-time state-space model for the full-order system described by equation (1). If a model reduction is performed, i.e. if the dynamics of the system are represented by a reduced number n_m of modal coordinates $\mathbf{z}(t) \in \mathbb{R}^{n_\mathrm{m}}$ as $\mathbf{u}(t) = \mathbf{\Phi}_\mathrm{r}\mathbf{z}(t)$, $\mathbf{\Phi}_\mathrm{r} \in \mathbb{R}^{n_\mathrm{DOF} \times n_\mathrm{m}}$, the state vector is transformed accordingly:

$$\mathbf{x}(t) = \begin{bmatrix} \mathbf{\Phi}_\mathrm{r} & \mathbf{0} \\ \mathbf{0} & \mathbf{\Phi}_\mathrm{r} \end{bmatrix} \boldsymbol{\zeta}(t).$$

The modal state vector $\boldsymbol{\zeta}(t) \in \mathbb{R}^{2n_\mathrm{m}}$ now collects the modal coordinates:

$$\boldsymbol{\zeta}(t) = \begin{pmatrix} \mathbf{z}(t) \\ \dot{\mathbf{z}}(t) \end{pmatrix}$$

and the expressions for the reduced-order continuous-time system matrices $\mathbf{A}_\mathrm{c} \in \mathbb{R}^{2n_\mathrm{m} \times 2n_\mathrm{m}}$, $\mathbf{B}_\mathrm{c} \in \mathbb{R}^{2n_\mathrm{m} \times n_\mathrm{p}}$, $\mathbf{G}_\mathrm{c} \in \mathbb{R}^{n_\mathrm{d} \times 2n_\mathrm{m}}$ and $\mathbf{J}_\mathrm{c} \in \mathbb{R}^{n_\mathrm{d} \times n_\mathrm{p}}$ in the modal state-space model:

$$\begin{aligned} \dot{\boldsymbol{\zeta}}(t) &= \mathbf{A}_\mathrm{c}\boldsymbol{\zeta} + \mathbf{B}_\mathrm{c}\mathbf{p}(t) && (7) \\ \mathbf{d}(t) &= \mathbf{G}_\mathrm{c}\boldsymbol{\zeta}(t) + \mathbf{J}_\mathrm{c}\mathbf{p}(t) && (8) \end{aligned}$$

can be shown to reduce to:

$$\begin{aligned} \mathbf{A}_\mathrm{c} &= \begin{bmatrix} \mathbf{0} & \mathbf{I} \\ -\mathbf{\Omega}^2 & -\mathbf{\Gamma} \end{bmatrix} && (9) \\ \mathbf{B}_\mathrm{c} &= \begin{bmatrix} \mathbf{0} \\ \mathbf{\Phi}^\mathrm{T}\mathbf{S}_\mathrm{p} \end{bmatrix} && (10) \\ \mathbf{G}_\mathrm{c} &= \begin{bmatrix} \mathbf{S}_\mathrm{d}\mathbf{\Phi} - \mathbf{S}_\mathrm{a}\mathbf{\Phi}\mathbf{\Omega}^2 & \mathbf{S}_\mathrm{v}\mathbf{\Phi} - \mathbf{S}_\mathrm{a}\mathbf{\Phi}\mathbf{\Gamma} \end{bmatrix} && (11) \\ \mathbf{J}_\mathrm{c} &= \left[\mathbf{S}_\mathrm{a}\mathbf{\Phi}\mathbf{\Phi}^\mathrm{T}\mathbf{S}_\mathrm{p}\right]. && (12) \end{aligned}$$

2.3 Discrete-time state-space model

Using a sampling rate of $1/\Delta t$, the state-space model of equations (4) and (6) - or the modal model of equations (7) and (8) - can be discretized to yield its discrete-time equivalent:

$$\begin{aligned} \mathbf{x}_{k+1} &= \mathbf{A}\mathbf{x}_k + \mathbf{B}\mathbf{p}_k && (13) \\ \mathbf{d}_k &= \mathbf{G}\mathbf{x}_k + \mathbf{J}\mathbf{p}_k && (14) \end{aligned}$$

where $\mathbf{x}_k = \mathbf{x}(k\Delta t)$, $\mathbf{d}_k = \mathbf{d}(k\Delta t)$, $k = 1, \ldots, N$ and:

$$\mathbf{A} = e^{\mathbf{A}_\mathrm{c}\Delta t},\ \mathbf{B} = [\mathbf{A} - \mathbf{I}]\mathbf{A}_\mathrm{c}^{-1}\mathbf{B}_\mathrm{c},\ \mathbf{G}_\mathrm{c} = \mathbf{G},\ \mathbf{J}_\mathrm{c} = \mathbf{J}.$$

3 JOINT INPUT-STATE ESTIMATION

In this section the joint input-state estimation algorithm developed by Gillijns and De Moor for linear systems with direct feedthrough of the unknown input to the output [6] is presented. Having direct feedthrough corresponds, from a structural dynamics point of view, to the situation where the measured quantities are accelerations, which is commonly the case. More details on the derivation of this algorithm and a proof of optimality, in a minimum-variance unbiased sense, can be found in [6].

The linear system under consideration is the discrete-time state-space system of equations (13) and (14), supplemented with random variables $\boldsymbol{w}_k$ and $\boldsymbol{v}_k$ representing the stochastic system and measurement noise, respectively:

$$\mathbf{x}_{k+1} = \mathbf{A}\mathbf{x}_k + \mathbf{B}\mathbf{p}_k + \boldsymbol{w}_k \tag{15}$$

$$\mathbf{d}_k = \mathbf{G}\mathbf{x}_k + \mathbf{J}\mathbf{p}_k + \boldsymbol{v}_k. \tag{16}$$

The noise vectors $\boldsymbol{w}_k \in \mathbb{R}^{n_\mathrm{s}}$ and $\boldsymbol{v}_k \in \mathbb{R}^{n_\mathrm{d}}$ are assumed to be mutually uncorrelated, zero-mean, white signals with known covariance matrices $\mathbf{Q} = \mathbb{E}\{\boldsymbol{w}_k\boldsymbol{w}_l^T\} \geq \mathbf{0}$ and $\mathbf{R} = \mathbb{E}\{\boldsymbol{v}_k\boldsymbol{v}_l^T\} > \mathbf{0}$. Results can easily be generalized to the case where $\mathbf{w}_k$ and $\mathbf{v}_k$ are correlated by applying a preliminary transformation to the system [1, 6]. Results can also be generalized to systems with both known and unknown inputs [6].

A state estimate $\hat{\mathbf{x}}_{k|l}$ is defined as an estimate of $\mathbf{x}_k$ given $\{\mathbf{d}_n\}_{n=0}^{l}$ and its error covariance matrix $\mathbf{P}_{k|l}$ as $\mathbb{E}[(\mathbf{x}_k - \hat{\mathbf{x}}_{k|l})(\mathbf{x}_k - \hat{\mathbf{x}}_{k|l})^T]$. An initial unbiased state estimate $\hat{\mathbf{x}}_{0|-1}$ and its covariance matrix $\mathbf{P}_{0|-1}$ is assumed known. The initial state estimate $\hat{\mathbf{x}}_0$ is assumed independent of $\mathbf{w}_k$ and $\mathbf{v}_k$ for all k. Finally, it is assumed that the rank of the direct transmission matrix $\mathbf{J}$ equals the number of applied forces n_p, and that the pair $(\mathbf{A}, \mathbf{G})$ is observable. It can be proven that the latter two assumptions are almost always valid when dealing with structural dynamic systems.

The filter is initialized using the initial state and its variance, $\hat{\mathbf{x}}_{0|-1}$ and $\mathbf{P}_{0|-1}$; hereafter it computes the force and state estimates recursively in three steps: the input estimation, the measurement update, and the time update:

Input estimation:

$$\tilde{\mathbf{R}}_{[k]} = \mathbf{G}\mathbf{P}_{[k|k-1]}\mathbf{G}^\mathrm{T} + \mathbf{R} \tag{17}$$

$$\boldsymbol{\mathcal{M}}_{[k]} = \left(\mathbf{J}^\mathrm{T}\tilde{\mathbf{R}}_{[k]}^{-1}\mathbf{J}\right)^{-1}\mathbf{J}^\mathrm{T}\tilde{\mathbf{R}}_{[k]}^{-1} \tag{18}$$

$$\hat{\mathbf{p}}_{[k|k]} = \boldsymbol{\mathcal{M}}_{[k]}\left(\mathbf{d}_{[k]} - \mathbf{G}\hat{\mathbf{x}}_{[k|k-1]}\right) \tag{19}$$

$$\mathbf{P}_{\mathbf{p}[k|k]} = \left(\mathbf{J}^\mathrm{T}\tilde{\mathbf{R}}_{[k]}^{-1}\mathbf{J}\right)^{-1} \tag{20}$$

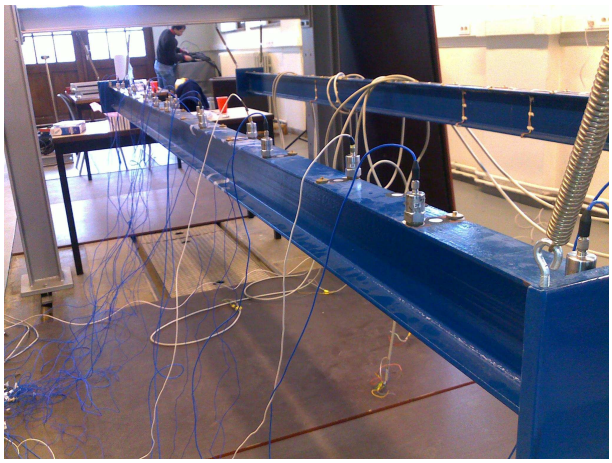

Figure 1: The measurement setup

Measurement update:

$$\mathbf{L}_{[k]} = \mathbf{P}_{[k|k-1]}\mathbf{G}^{\mathrm{T}}\tilde{\mathbf{R}}_{[k]}^{-1} \tag{21}$$

$$\hat{\mathbf{x}}_{[k|k]} = \hat{\mathbf{x}}_{[k|k-1]} + \mathbf{L}_{[k]}\left(\mathbf{d}_{[k]} - \mathbf{G}\hat{\mathbf{x}}_{[k|k-1]} - \mathbf{J}\mathbf{p}_{[k|k]}\right) \tag{22}$$

$$\mathbf{P}_{[k|k]} = \mathbf{P}_{[k|k-1]} - \mathbf{L}_{[k]}\left(\tilde{\mathbf{R}}_{[k]} - \mathbf{J}\mathbf{P}_{\mathbf{p}[k|k]}\mathbf{J}^{\mathrm{T}}\right)\mathbf{L}_{[k]}^{\mathrm{T}} \tag{23}$$

$$\mathbf{P}_{\mathbf{xp}[k|k]} = \mathbf{P}_{\mathbf{px}[k|k]}^{\mathrm{T}} = -\mathbf{L}_{[k]}\mathbf{J}\mathbf{P}_{\mathbf{p}[k|k]} \tag{24}$$

Time update:

$$\mathbf{x}_{[k+1|k]} = \mathbf{A}\hat{\mathbf{x}}_{[k|k]} + \mathbf{B}\hat{\mathbf{p}}_{[k|k]} \tag{25}$$

$$\mathbf{P}_{[k+1|k]} = \begin{bmatrix} \mathbf{A} & \mathbf{B} \end{bmatrix} \begin{bmatrix} \mathbf{P}_{[k|k]} & \mathbf{P}_{\mathbf{xp}[k|k]} \\ \mathbf{P}_{\mathbf{px}[k|k]} & \mathbf{P}_{\mathbf{p}[k|k]} \end{bmatrix} \begin{bmatrix} \mathbf{A}^{\mathrm{T}} \\ \mathbf{B}^{\mathrm{T}} \end{bmatrix} + \mathbf{Q} \tag{26}$$

It is mentioned that when $\mathbf{B} = \mathbf{J} = \mathbf{0}$, the Kalman filter is obtained. In the above, the system matrices are for ease of notation not indexed. The algorithm can, however, also be applied to time-variant systems by simply adding the appropriate subscripts, i.e. $\mathbf{A}_k$, $\mathbf{B}_k$, $\mathbf{G}_k$ and $\mathbf{J}_k$.

4 EXPERIMENTAL RESULTS

In this section the effectiveness of the proposed algorithm is illustrated by means of a laboratory experiment on an instrumented steel beam as well as an in situ experiment on a footbridge.

4.1 Laboratory experiment on a steel beam

A steel beam with an IPE100 cross section, a length of 3m, and plates of 150x150x15 mm welded to its ends, is suspended at both ends from a steel frame using flexible springs to simulate free-free boundary conditions. A series of accelerometers is placed along the beam to record its response to an impact force, applied with an instrumented hammer. The aim here is to use a subset of the measured accelerations to identify the remaining (measured) accelerations.

Vertical accelerations on the top flange of the beam were measured at 17 different cross sections using 19 accelerometers (PCB 338B35, sensitivity $\pm$ 100 mV/g). The force was applied eccentrically with an impact hammer (PCB 086C03, mass 0.136 kg) at one of the free-free beam

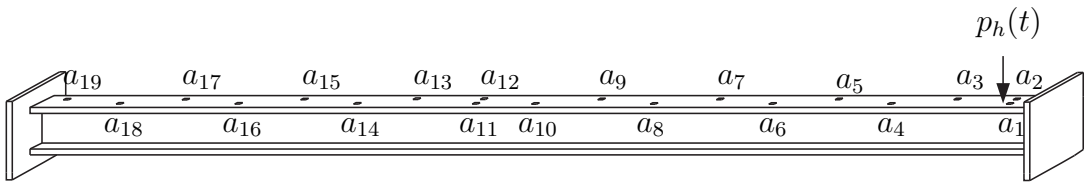

Figure 2: Positions of the sensors and applied force.

ends. The measurement setup and positions of the sensors and applied force are shown in figures 1 and 2. The modal parameters of the beam were identified in a Operational Modal Analysis with eXogenous inputs (OMAX) test [13] for the frequency range $0 - 900$ Hz. More details on this test and its results can be found in [10]. The identified modal parameters were used to tune the Young's modulus of the steel and the stiffness of the springs in a FE model. A comparison between the identified and computed eigenmodes is shown in table 1. Except for the torsional modes, whose contribution to the acceleration response considered is almost negligible, a good correspondence is found between the measured and experimental eigenfrequencies. All modes are very lightly damped with damping ratios below 0.5 % of critical.

	FEM	Experimental		
	f_{udi}	f_{udi}	ξ_i	MAC
No.	[Hz]	[Hz]	[%]	[−]
1	1.780	1.771	0.36	0.99
2	2.787	2.701	0.19	1.00
3	3.106	4.917	0.41	0.99
4	31.56	30.81	0.12	0.99
5	61.51	60.90	0.05	1.00
6	74.94	71.20	0.32	0.98
7	136.0	128.1	0.15	0.99
8	174.6	173.9	0.04	1.00
9	216.9	200.5	0.12	0.98
10	319.1	293.5	0.13	0.97
11	341.9	341.0	0.02	1.00
12	443.3	402.6	0.11	0.98
13	589.8	535.4	0.12	0.95
14	557.4	556.7	0.03	1.00
15	807.1	805.6	0.04	1.00

Table 1: Comparison between the undamped eigenfrequencies f_{udi} of the FE model of the beam and those that were experimentally obtained. The experimental damping ratios ξ_i and MAC values between the measured mass-normalized mode shapes and the ones obtained from the FE model, are shown as well.

The 15 modes from the FE model, consisting of 3 rigid body, 5 bending and 7 torsional modes, are used to construct a reduced-order modal state-space model of the beam. Originally sampled at 10 kHz, all data used in the inverse calculations are resampled at a lower rate in order to include only frequencies within the range of the identified modes. Using a decimation factor of 5, the data is low-pass filtered using a Chebychev Type I filter at 800Hz and subsequently resampled at 2 kHz.

Of the 19 measured accelerations, 10 are used to identify the modal states and input forces, from which the acceleration (or displacement, strain, etc.) at any other point in the structure can be calculated as $\hat{\mathbf{d}} = \mathbf{G}\hat{\mathbf{x}} + \mathbf{J}\hat{\mathbf{p}}$. It is assumed that no a priori information on the positions of the forces is available and a set of equivalent forces are assumed to act at all measurement locations used for the identification, i.e. at positions a_1, a_3, a_4, a_6, a_9, a_{11}, a_{15}, a_{17}, a_{18} and a_{19}. The accelerations identified at the remaining locations are compared to the measured data during a period of 1 s. The covariance matrices $\mathbf{Q}$, $\mathbf{R}$ and $\mathbf{P}_{0|-1}$ are assigned values of $1e^{-10}$, $1e^{-1}$ and $1e^{-10}$ on the diagonal, respectively. In accordance with what they represent, these values are chosen so as to have the order of the square roots of the diagonal elements of $\mathbf{R}$ and $\mathbf{Q}$ corresponding to a small percentage of the highest peaks in the measured response and the states (displacements/velocities), respectively. The small values in $\mathbf{P}_{0|-1}$ indicate a low level of uncertainty regarding the initial state estimate. It is mentioned that the results are, however, not strongly influenced by these values and similar results are obtained for a large range of $\mathbf{Q}$, $\mathbf{R}$ and $\mathbf{P}_{0|-1}$.

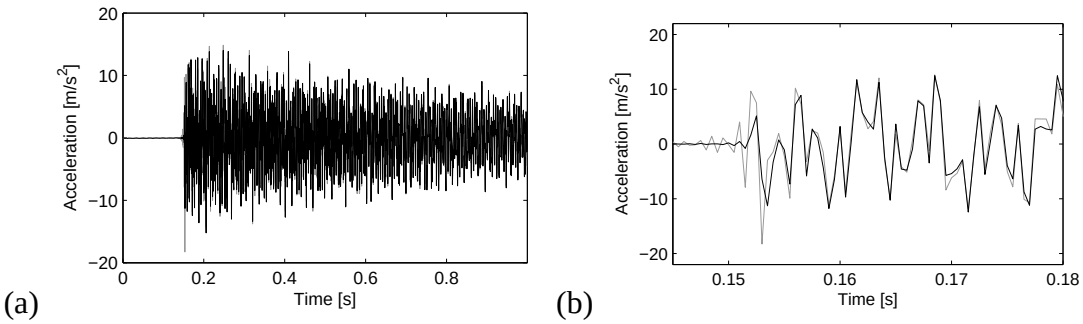

(a) (b)

Figure 3: a) Complete and b) detail of the measured (black) and identified (grey) time history of the acceleration at sensor a_7.

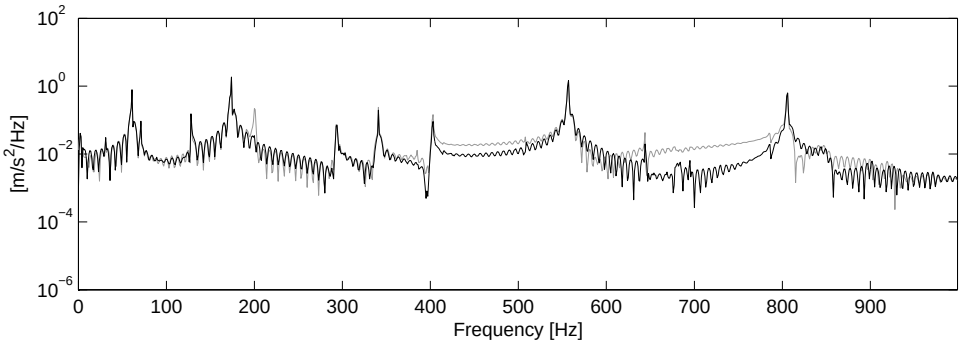

Figure 4: Frequency spectrum of the measured (black) and identified (grey) acceleration at sensor a_7.

Figures 3 to 8 show the results obtained when the beam is excited with the hammer at $t = \pm 0.15s$. Measured accelerations are plotted against those identified for three randomly chosen locations, namely a_7, a_{13} and a_{16}. The accelerations are compared in the time as well as in the frequency domain, and a detail of the acceleration time history at the time of impact is presented as well. A good reconstruction is obtained at all 3 locations.

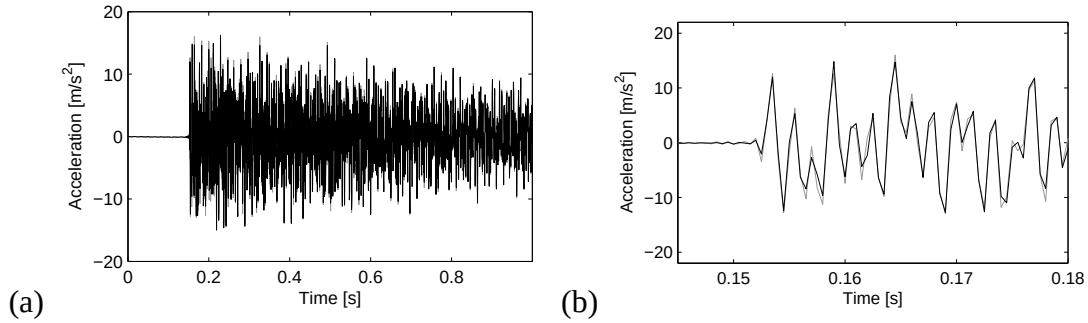

Figure 5: a) Complete and b) detail of the measured (black) and identified (grey) time history of the acceleration at sensor a_{13}.

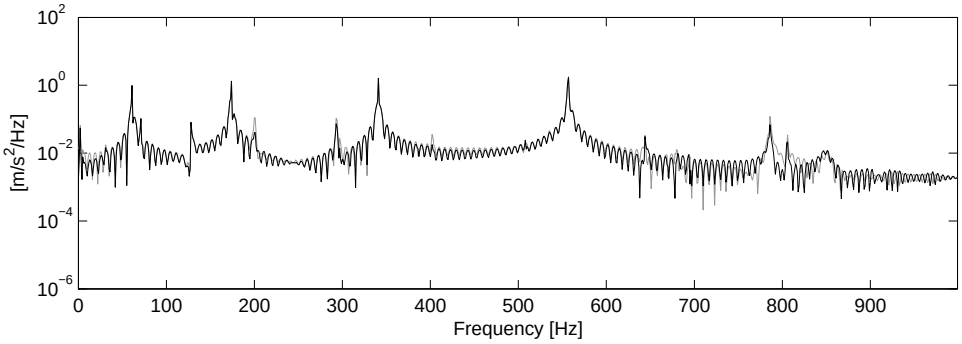

Figure 6: Frequency spectrum of the measured (black) and identified (grey) acceleration at sensor a_{13}.

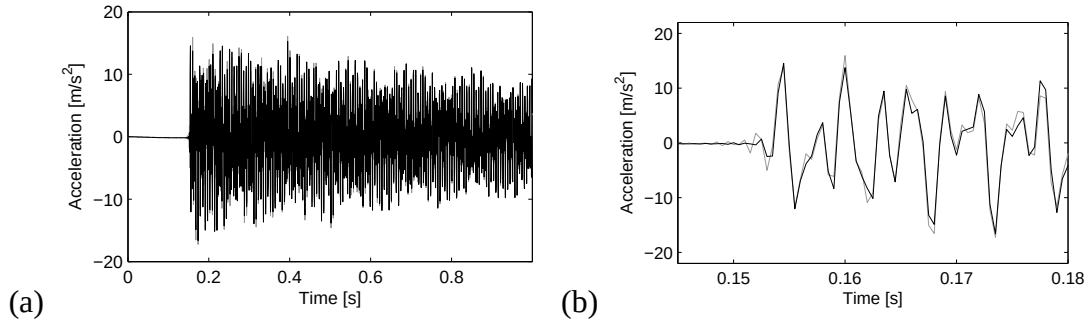

Figure 7: a) Complete and b) detail of the measured (black) and identified (grey) time history of the acceleration at sensor a_{16}.

4.2 In situ experiment on a footbridge

Analogous to the previous test case, a subset of the accelerations measured during an in situ test on a footbridge is used to identify modal states and a set of equivalent forces. The identified modal states and forces are subsequently used to calculate the accelerations at the remaining measured positions and a comparison is made. The footbridge, depicted in figure 9, is located in Wetteren (Belgium), and has been used as an in situ test case for Operational Modal Analysis (OMA) [12] and previously mentioned OMAX techniques. It is a steel bridge that crosses the E40 highway between Brussels and Ghent at Wetteren, with a short and long bow-string span of 30.33m and 75.23m, respectively.

For the OMAX tests, measurements have been performed in a total number of 72 channels

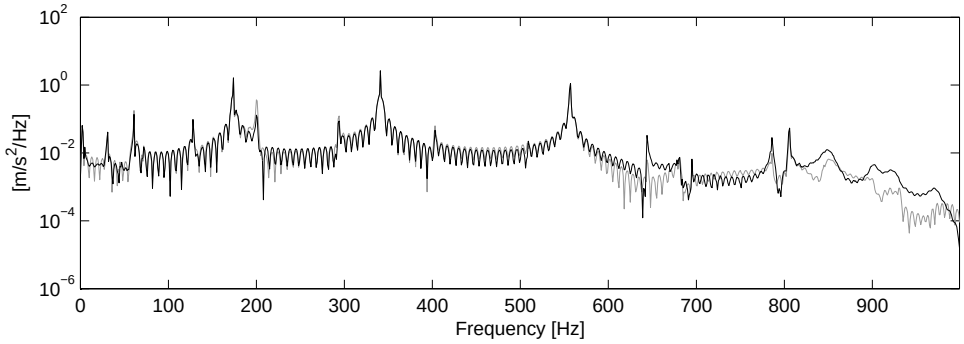

Figure 8: Frequency spectrum of the measured (black) and identified (grey) acceleration at sensor a_{16}.

Figure 9: The footbridge in Wetteren, Belgium.

during different setups. The locations of the sensors are shown in figure 10. The data used in the current example was obtained during excitation of the bridge by means of a drop weight system. The drop weight was applied at point 34, in the vertical direction, and during the setup accelerations were measured in 16 channels. In the following, 8 of the measured accelerations will be used to identify the modal states and to reconstruct the accelerations at the 8 remaining locations. Equivalent loads are assumed to act in the directions and at the locations of the 8 measured accelerations. The actual load on the structure consists of the drop weight as well as a high level of ambient excitation due to traffic underneath the bridge and wind.

Of the 16 measured accelerations, 4 vertical and 4 lateral accelerations were identified as optimal for the identification. These are the vertical accelerations in points 2, 3, 24 and 34 on the bridge deck, the lateral accelerations on the bridge deck at points 14 and 19, and the lateral accelerations of the bow at points 45 and 48. With the optimal 8 accelerations as input, the proposed algorithm is used to identify 7 'unmeasured' vertical accelerations at points 8, 12, 14, 25, 30, 36 and 41 on the bridge deck, and the lateral acceleration at point 12 on the bow.

The system matrices are constructed from an updated finite element (FE) model of the bridge. In the FE model, developed using the FE program ANSYS, the bridge deck is modeled using the ANSYS shell element SHELL63. The longitudinal and transversal beams of the bridge deck, as well as the bows, connections of the bows, and supports, are modeled using the beam element BEAM188. A 3D truss element, LINK8, is used to model the cables, taking into account the effective stiffness E_{eff} of the cable based on the tensile cable force. The model has a total of

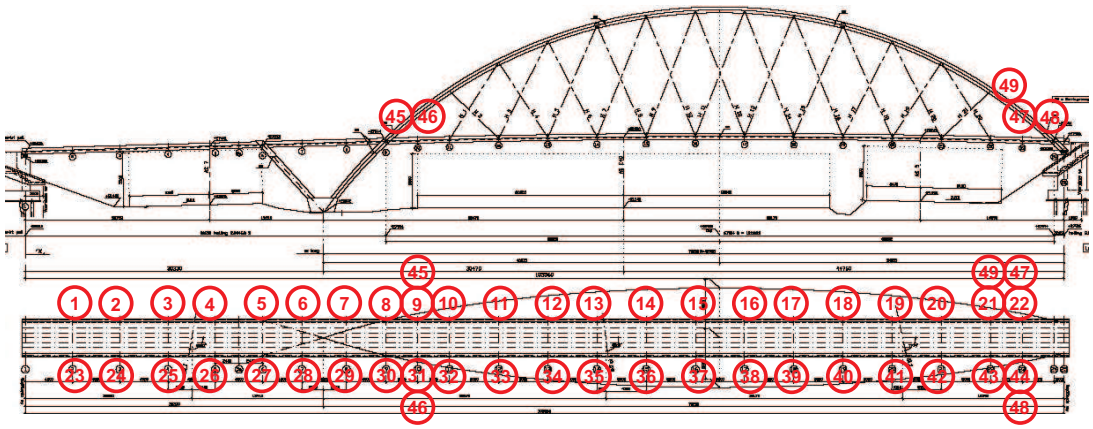

Figure 10: Positions of the sensors.

16007 nodes and 2210 elements. The first 4 modes calculated with the model are shown in figure 11.

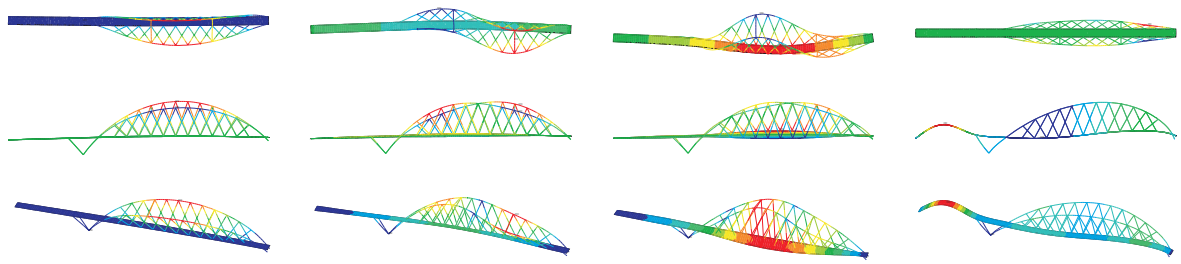

Figure 11: Results from the FE modal analysis for the first 4 modes. Top: transversal displacements, middle: vertical displacements, bottom: displacement vector sum.

The FE model is updated using a set of experimental modal parameters obtained during an OMAX test [14] in which the actuator was a pneumatic artificial muscle (PAM) developed by the Acoustics and Vibration Research Group of the Vrije Universiteit Brussel [4]. Table 2 presents a comparison between the eigenfrequencies of the updated FE model and those that were identified experimentally. The experimental damping ratios as well as the MAC values between the mass-normalized mode shapes and the ones obtained from the FE model are shown in the table. The 22 eigenmodes of the FE model, in conjunction with the corresponding identified modal damping ratios, are used to construct a reduced-order modal state-space model of the structure. As before, all data used in the inverse calculations are resampled at a lower rate. Using a decimation factor of 23, the data is low-pass filtered using a Chebychev Type I filter at 17.39 Hz and subsequently resampled at 43.48 Hz. A period of 9 s, in which the impact from the drop-weight is applied at $t = 2.3$ s, is analysed.

As in the previous examples equivalent forces are assumed to act at all measurement locations. The covariance matrices $\mathbf{Q}$, $\mathbf{R}$ and $\mathbf{P}_{0|-1}$ are assigned values of $1e^{-10}$, $1e^{-1}$ and $1e^{-10}$ on the diagonal, respectively. In figures 12 to 15, 4 of the 8 identified accelerations are compared to those measured. The results are for the vertical accelerations at points 12, 25 and 41 (figures 12 to 14), and the lateral acceleration at point 12 (figure 15).

The identified accelerations are of lesser quality than those in the laboratory experiment, which can partly be explained by the fact that the updated FE model of the footbridge represents the structure considerably less accurately than the one used in the laboratory experiment (cfr.

	FEM	Experimental				FEM	Experimental		
	f_{udi}	f_{udi}	ξ_i	MAC		f_{udi}	f_{udi}	ξ_i	MAC
No.	[Hz]	[Hz]	[%]	[−]	No.	[Hz]	[Hz]	[%]	[−]
1	0.739	0.693	1.05	0.92	12	8.599	8.307	1.18	0.79
2	1.739	1.669	0.23	0.87	13	10.395	9.967	1.10	0.65
3	2.363	2.195	0.50	0.98	14	11.397	10.475	0.64	0.76
4	3.250	3.731	0.55	0.71	15	11.864	11.214	0.78	0.85
5	3.833	3.838	0.49	0.80	16	11.625	11.821	1.68	0.79
6	4.897	4.480	0.76	0.84	17	13.147	12.728	0.35	0.70
7	5.370	5.154	0.44	0.86	18	13.255	12.863	0.72	0.89
8	6.377	6.117	0.27	0.88	19	14.479	13.530	0.72	0.62
9	6.662	6.321	0.50	0.92	20	15.312	14.810	0.41	0.80
10	6.991	6.605	0.58	0.88	21	16.648	16.502	0.53	0.82
11	8.028	7.488	0.70	0.82	22	18.358	17.833	0.28	0.88

Table 2: Comparison between the undamped eigenfrequencies f_{udi} of the updated FE model and those that were experimentally obtained in an OMAX test using the PAM. The experimental damping ratios ξ_i and MAC values between the measured mass-normalized mode shapes and the ones obtained from the FE model, are shown as well.

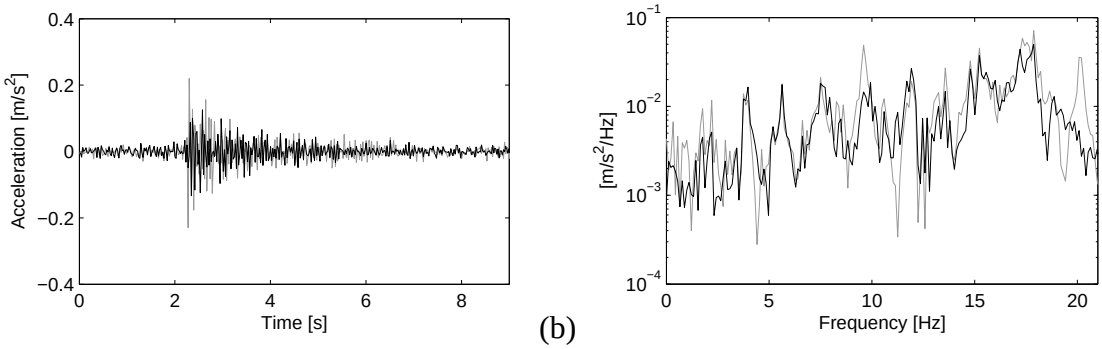

(a) (b)

Figure 12: a) Time history and b) frequency spectrum of the measured (black) and identified (grey) vertical acceleration at point 12.

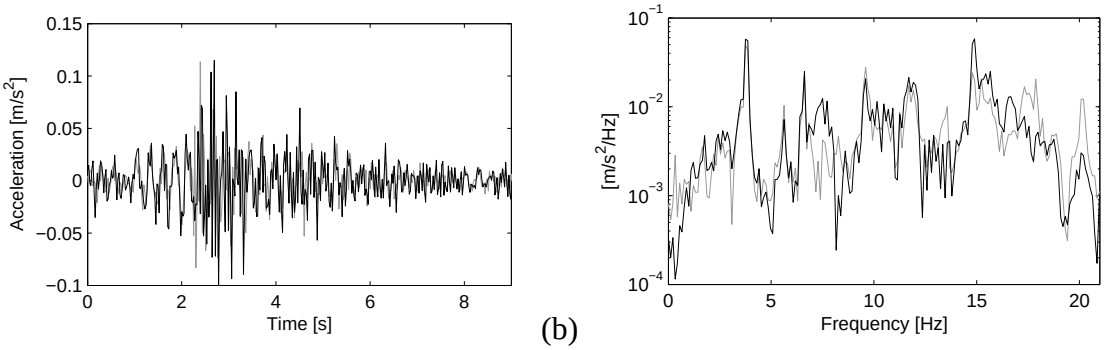

(a) (b)

Figure 13: a) Time history and b) frequency spectrum of the measured (black) and identified (grey) vertical acceleration at point 25.

MAC values in tables 1 and 2). Also, the number of sensors used is small compared to the geometrical and modal complexity of the footbridge. Taking these circumstances into account

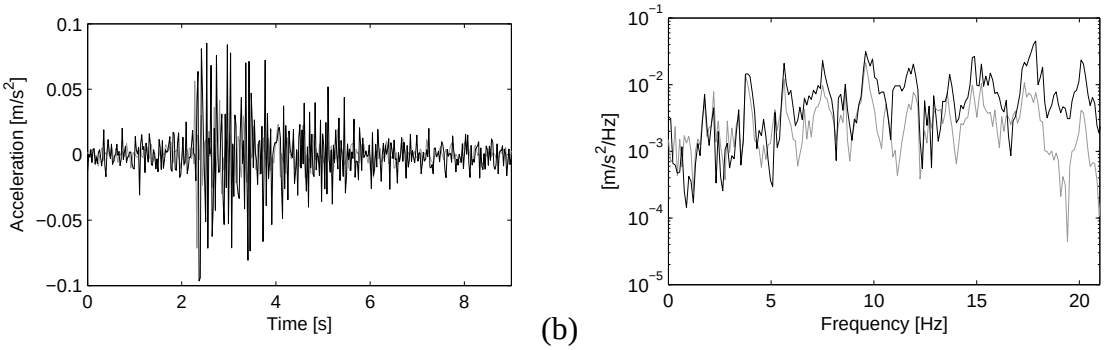

(a) (b)

Figure 14: a) Time history and b) frequency spectrum of the measured (black) and identified (grey) vertical acceleration at point 41.

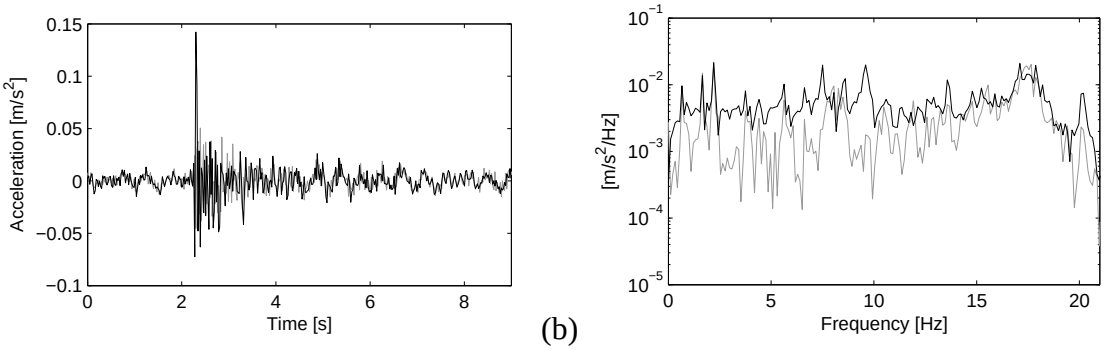

(a) (b)

Figure 15: a) Time history and b) frequency spectrum of the measured (black) and identified (grey) lateral acceleration at point 12.

the identification is in fact very reasonable, especially those in the vertical direction. Moreover, the accuracy of the identification is similar for both the ambient part of the acceleration from $t = 0 - 2.3\ s$, where the vibrations are caused by low amplitude traffic loads, and the remaining stronger intensity part of the acceleration caused by the drop weight. The identification of the lateral acceleration is considerably less good between the resonance frequencies (cfr. figure 15b), but the dominant frequency components are still well identified. It can be concluded that the proposed algorithm performs well even when a significant amount of modeling error is present.

5 CONCLUSIONS

An existing model-based joint input-state estimation algorithm requiring no prior information on the dynamic evolution of the input forces, was used to estimate the state of a structure from a limited number of acceleration measurements. The algorithm's accuracy and applicability were tested using data from a laboratory experiment on an instrumented steel beam as well as an in situ experiment on a footbridge. It is concluded that the algorithm is capable of accurately estimating the state of a structure from a limited number of noise-contaminated acceleration measurements, also when a relatively high level of modeling error is present and no prior information on the positions or nature of the input forces is available.

REFERENCES

[1] B.D.O. Anderson and J.B. Moore. *Optimal filtering*. Prentice Hall, Englewood Cliffs, New Jersey, 1979.

[2] J. Ching and J.L. Beck. Real-time reliability estimation for serviceability limit states in structures with uncertain dynamic excitation and incomplete output data. *Probabilistic Engineering Mechanics*, 22:50–62, 2007.

[3] J. Ching, J.L. Beck, and K.A. Porter. Bayesian state and parameter estimation of uncertain dynamical systems. *Probabilistic Engineering Mechanics*, 21:81–96, 2006.

[4] K. Deckers, P. Guillaume, D. Lefeber, G. De Roeck, and E. Reynders. Modal testing of bridges using low-weight pneumatic artificial muscle actuators. In *Proceedings of IMAC 26, the International Modal Analysis Conference*, Orlando, FL, February 2008. CD-ROM.

[5] R.G. Ghanem and P.D. Spanos. *Stochastic finite elements: a spectral approach*. Springer-Verlag, New York, 1991.

[6] S. Gillijns and B. De Moor. Unbiased minimum-variance input and state estimation for linear discrete-time systems with direct feedthrough. *Automatica*, 43:934–937, 2007.

[7] E.M. Hernandez and D. Bernal. An observer-based approach for model updating. In *Proceedings of IMAC XXIV International Modal Analysis Conference*, 2006.

[8] E.M. Hernandez and D. Bernal. State estimation in nonlinear structural systems with model uncertainties. In *Proceedings of IMAC XXV International Modal Analysis Conference*, 2007.

[9] E.M. Hernandez and D. Bernal. State estimation in structural systems with model uncertainties. *ASCE Journal of Engineering Mechanics*, 134(3):252–257, 2008.

[10] E. Lourens, E. Reynders, G. Lombaert, G. De Roeck, and G. Degrande. Dynamic force identification by means of state-augmentation: a combined deterministic-stochastic approach. In *Proceedings of ISMA2010 International Conference on Noise and Vibration Engineering*, pages 2069–2080, Leuven, Belgium, September 2010.

[11] C. Papadimitriou, C.-P. Fritzen, P. Kraemer, and E. Ntotsios. Fatigue predictions in entire body of metallic structures from a limited number of vibration sensors using kalman filtering. *Structural Control and Health Monitoring*, 2011. Published online in Wiley InterScience (www.interscience.wiley.com). DOI:10.1002/stc.395.

[12] B. Peeters and G. De Roeck. Reference-based stochastic subspace identification for output-only modal analysis. *Mechanical Systems and Signal Processing*, 13(6):855–878, 1999.

[13] E. Reynders and G. De Roeck. Reference-based combined deterministic-stochastic subspace identification for experimental and operational modal analysis. *Mechanical Systems and Signal Processing*, 22(3):617–637, 2008.

[14] E. Reynders, D. Degrauwe, G. De Roeck, F. Magalhães, and E. Caetano. Combined experimental-operational modal testing of footbridges. *ASCE Journal of Engineering Mechanics*, 136(6):687–696, 2010.

[15] A. Smyth and M. Wu. Multi-rate kalman filtering for the data fusion of displacement and acceleration response measurements in dynamic system monitoring. *Mechanical Systems and Signal Processing*, 21:706–723, 2007.